Science Advances
AAAS

Supplementary Materials for

Large slip, long duration, and moderate shaking of the Nicaragua 1992 tsunami earthquake caused by low near-trench rock rigidity

Valentí Sallarès*, Manel Prada, Sebastián Riquelme, Adrià Meléndez, Alcinoe Calahorrano, Ingo Grevemeyer, César R. Ranero

*Corresponding author. Email: vsallares@icm.csic.es

Published 6 August 2021, *Sci. Adv.* **7**, eabg8659 (2021)
DOI: 10.1126/sciadv.abg8659

This PDF file includes:

Figs. S1 to S12

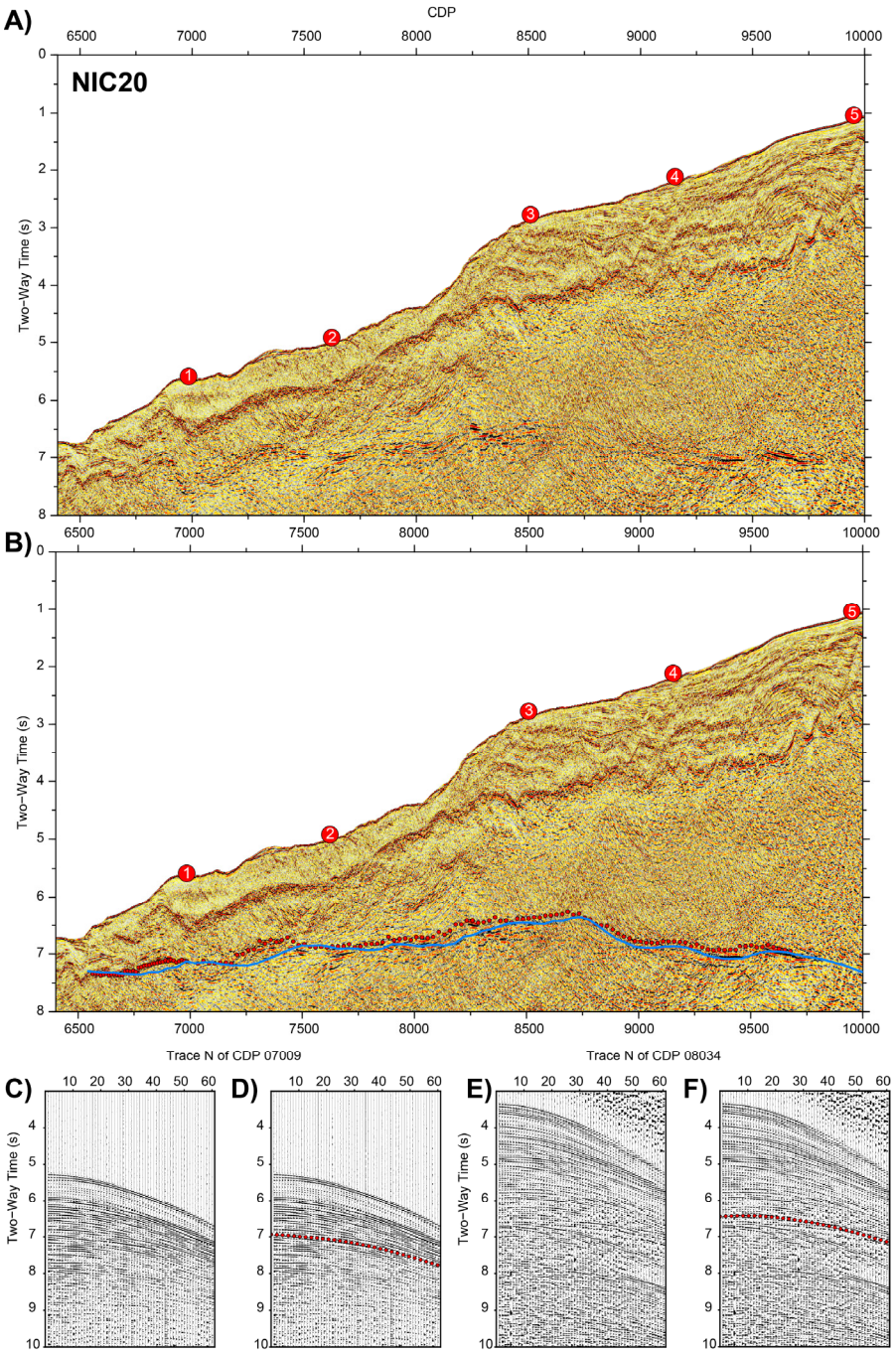

Fig. S1. MCS data along NIC20 profile. (A) Un-interpreted and **(B)** interpreted versions of the stacked data along the NIC20 MCS profile (see location in Fig. 1A). Large numbered circles indicate OBS locations. Small red circles indicate P_iP travel-times picked in each CDP. Blue line is the TWT-converted reflector obtained by joint refraction and reflection travel-time tomography. CDP spacing along the line is 12.5 m. **(C)** Un-interpreted and **(D)** interpreted versions of the CDP gather # 7009 along the NIC20 MCS profile. **(E)** Un-interpreted, and **(F)** interpreted versions of the CDP gather # 8034 along the NIC20 MCS profile. Red circles in D) and F) show the picked inter-plate boundary reflector. Trace distance at the CDP gathers is 100 m.

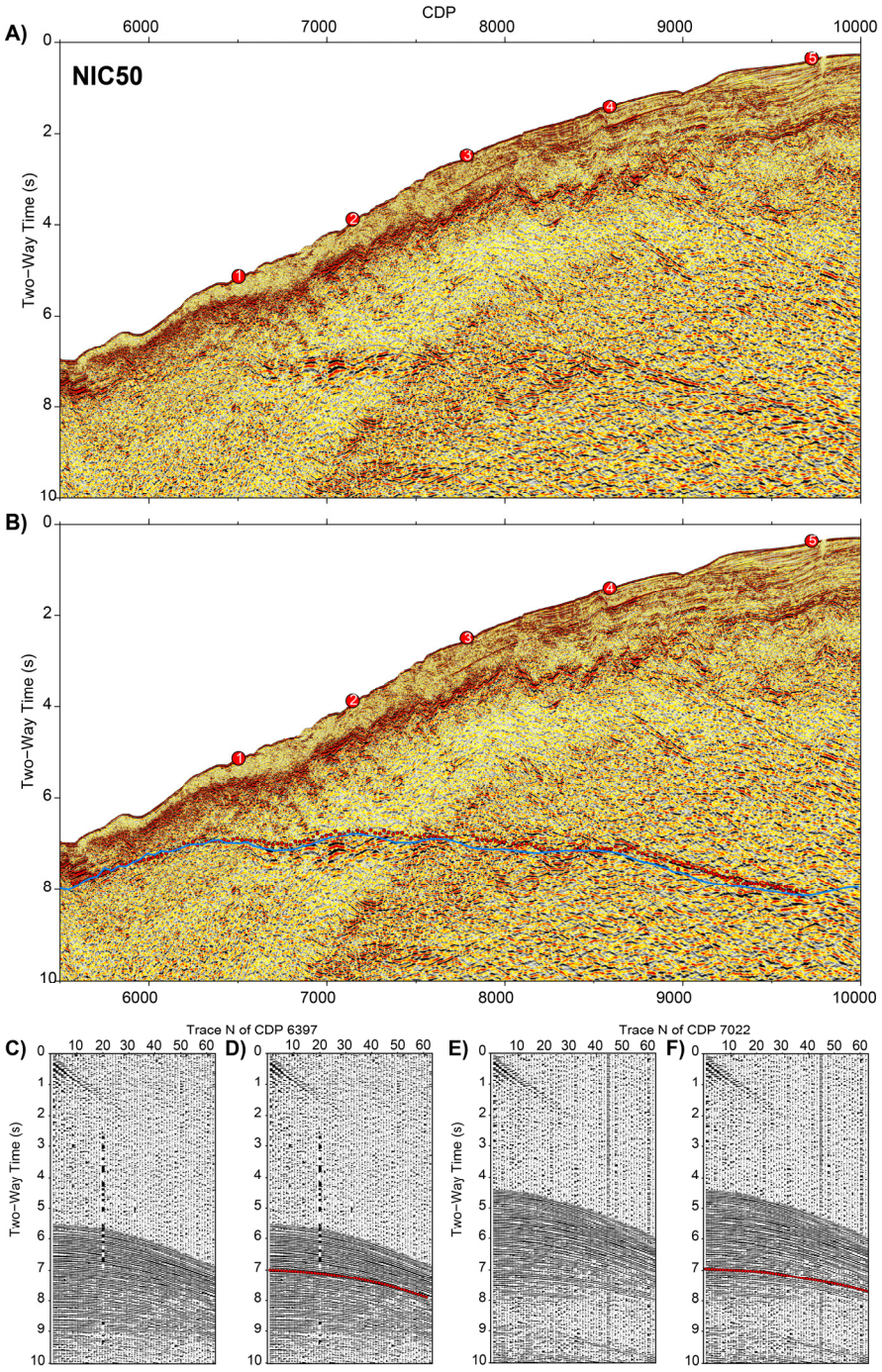

Fig. S2. MCS data along NIC50 profile. (A) Un-interpreted and **(B)** interpreted versions of the stacked data along the NIC50 MCS profile (see location in Fig. 1A). Large numbered circles indicate OBS locations. Small red circles indicate P_iP travel-times picked in each CDP. Blue line is the TWT-converted reflector obtained by joint refraction and reflection travel-time tomography. CDP spacing along the line is 12.5 m. **(C)** Un-interpreted and **(D)** interpreted versions of the CDP gather # 6397 along the NIC50 MCS profile. **(E)** Un-interpreted and **(F)** interpreted versions of the CDP gather # 7022 along the NIC50 MCS profile. Red circles in D) and F) show the picked inter-plate boundary reflector. Trace distance at the CDP gathers is 100 m.

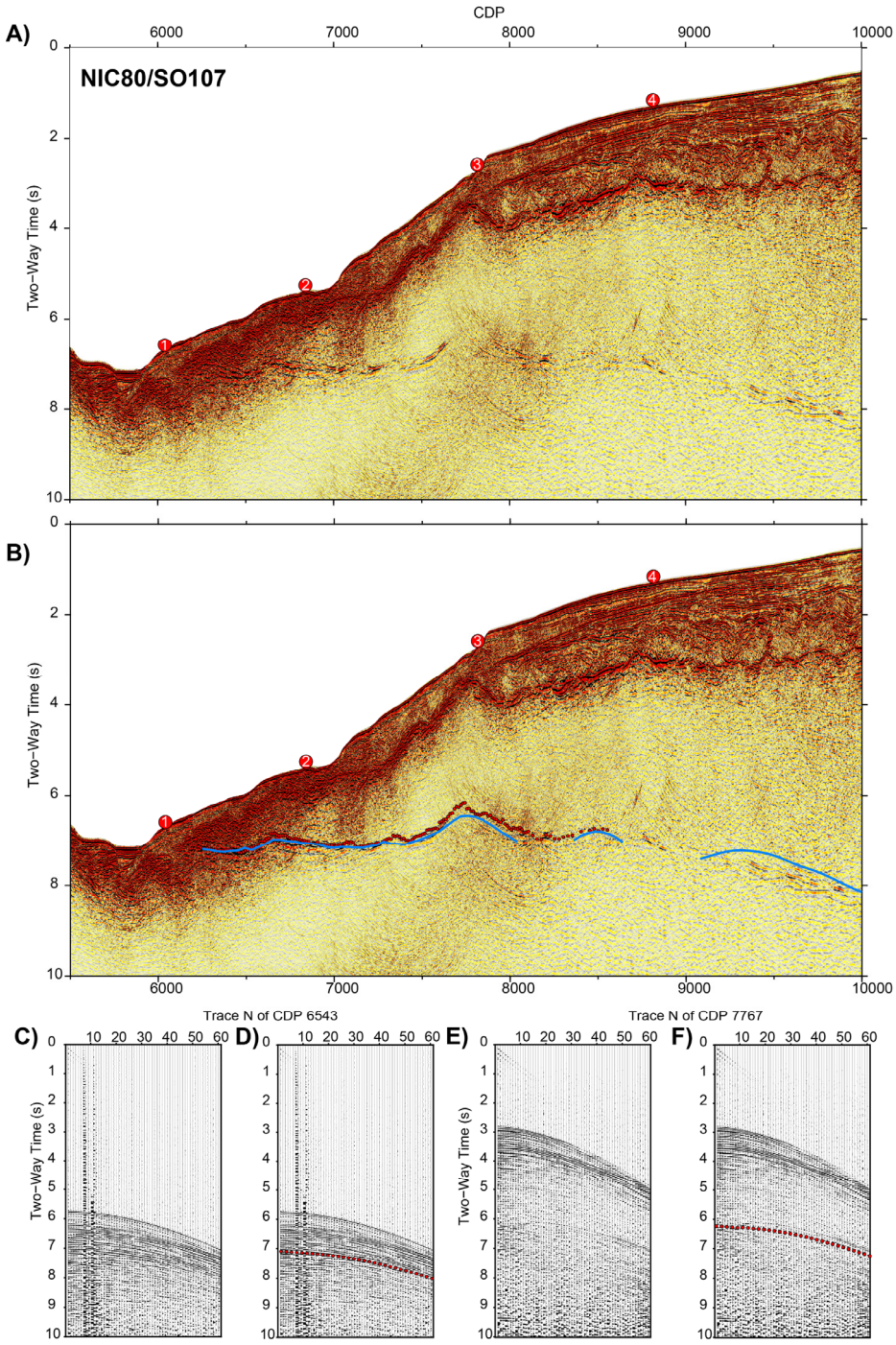

Fig. S3. MCS data along NIC80/SO107 profile. (A) Un-interpreted and **(B)** interpreted versions of the stacked data along the NIC80/SO107 MCS profile (see location in Fig. 1A). Large numbered circles indicate OBS locations. Small red circles indicate P_iP travel-times picked in each CDP.Blue line is the TWT-converted reflector obtained by joint refraction and reflection travel-time tomography. CDP spacing along the line is 12.5 m. **(C)** Un-interpreted and **(D)** interpreted versions of the CDP gather # 6543 along the NIC80/SO107 MCS profile. (**E)** Un-interpreted, and **(F)** interpreted versions of the CDP gather # 7767 along the NIC80/SO107 MCS profile. Red circles in D) and F) show the picked inter-plate boundary reflector. Trace distance at the CDP gathers is 100 m.

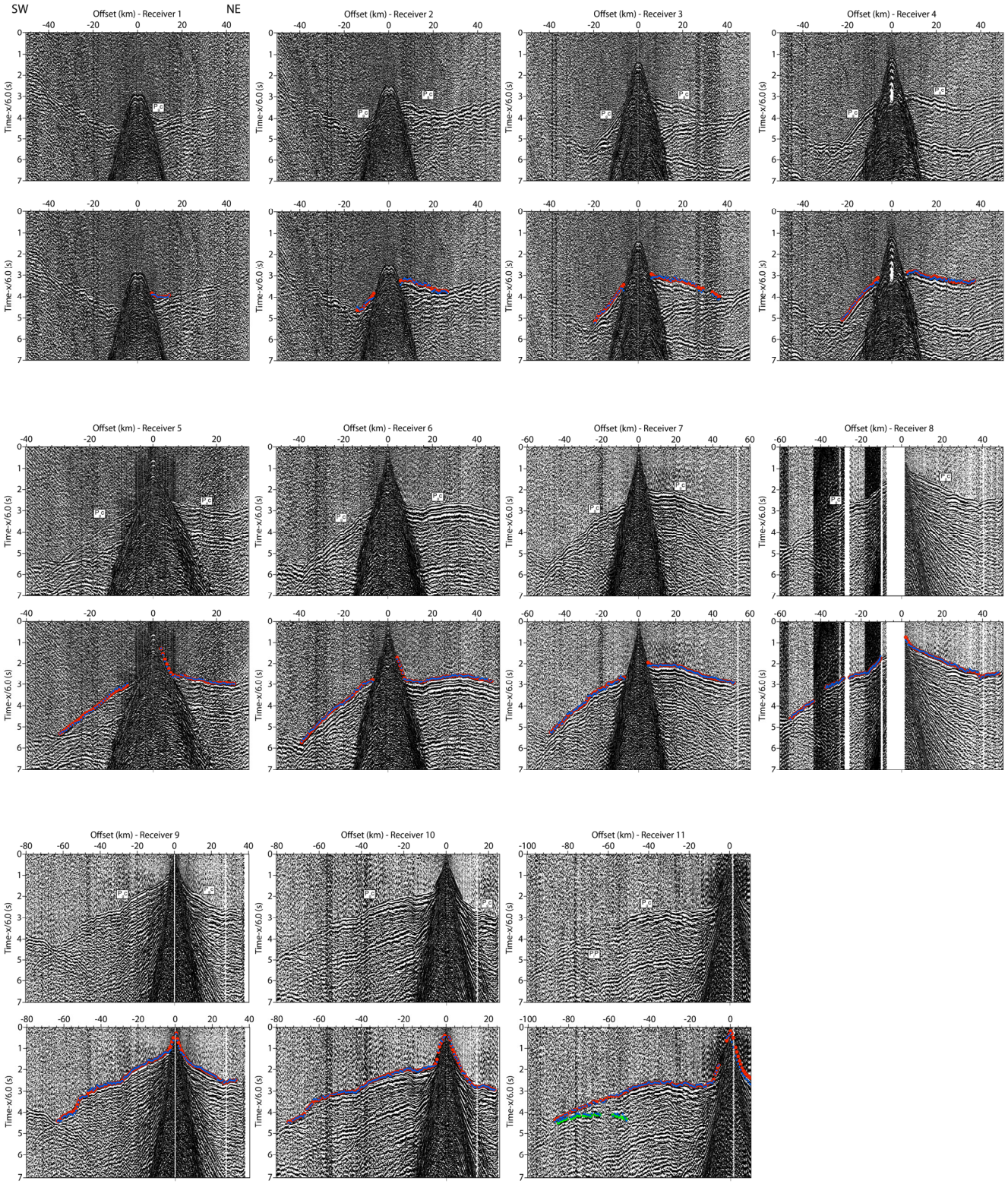
SW
NE
Offset (km) - Receiver 1
Offset (km) - Receiver 2
Offset (km) - Receiver 3
Offset (km) - Receiver 4
Offset (km) - Receiver 5
Offset (km) - Receiver 6
Offset (km) - Receiver 7
Offset (km) - Receiver 8
Offset (km) - Receiver 9
Offset (km) - Receiver 10
Offset (km) - Receiver 11
Time-x/6.0 (s)
PG
PG

(previous page)

Fig. S4. OBH data along NIC20 profile. Record sections acquired at OBHs 1-11 along the WAS profile NIC20 (see location in Fig. 1A). Red circles are the first arrival picks of refracted waves travelling through the upper plate (P_{gc}), whereas green circles are the inter-plate boundary reflection picks (P_iP). Blue circles correspond to the inverted travel-time picks for both P_{gc} and P_iP phases. Reduction velocity is 6 km s^{-1} in all the record sections.

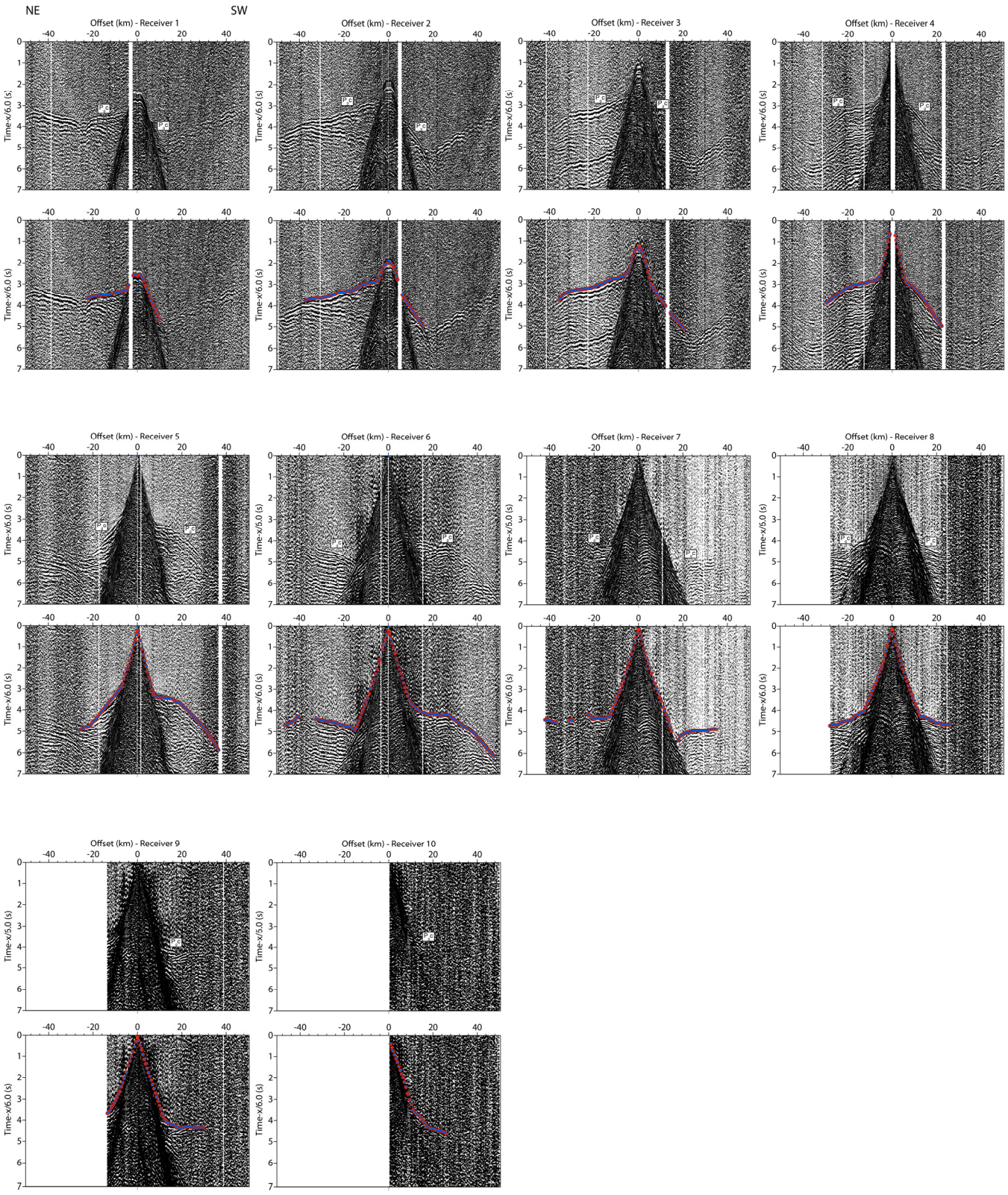
NE
SW
Offset (km) - Receiver 1
Offset (km) - Receiver 2
Offset (km) - Receiver 3
Offset (km) - Receiver 4
Offset (km) - Receiver 5
Offset (km) - Receiver 6
Offset (km) - Receiver 7
Offset (km) - Receiver 8
Offset (km) - Receiver 9
Offset (km) - Receiver 10
Time-x/6.0 (s)
Time-x/5.0 (s)
-40
-20
0
20
40
0
1
2
3
4
5
6
7
PG

(previous page)

Fig. S5. OBH data along NIC50 profile. Record sections acquired at OBHs 1-8 along the WAS profile NIC50 (see location in Fig. 1A). Red circles are the first arrival picks of refracted waves travelling through the upper plate (P_{gc}). Blue circles correspond to the inverted travel-time picks for P_{gc} phases. Reduction velocity is 6 km s^{-1} in all the record sections.

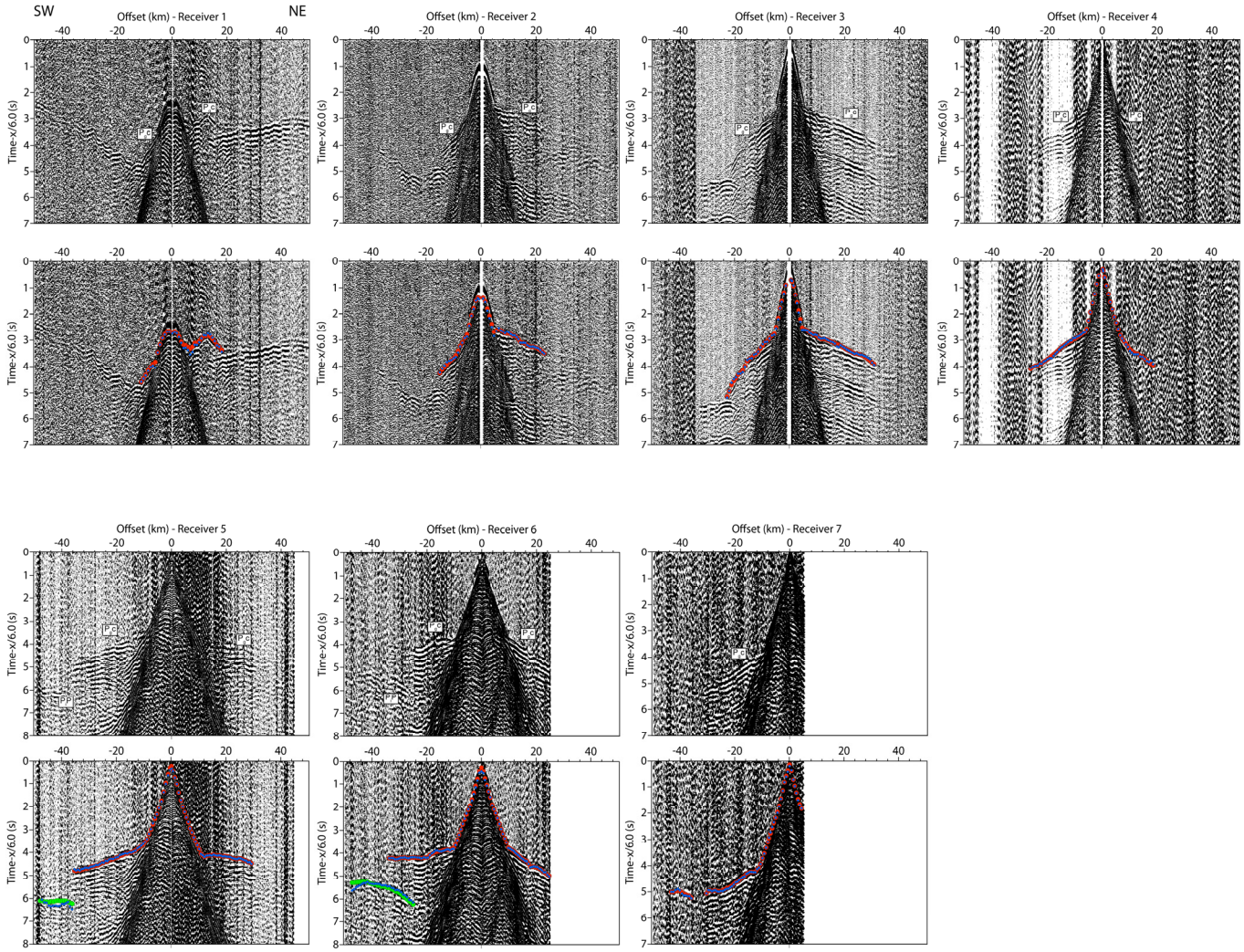

Fig. S6. OBH data along NIC80/SO107 profile. Record sections acquired at OBHs 1-7 along the WAS profile NIC80/SO107 (see location in Fig. 1A). Red circles are the first arrival picks of refracted waves travelling through the upper plate (P_{gc}), whereas green circles are the inter-plate boundary reflection picks (P_iP). Blue circles correspond to the inverted travel-time picks for both P_{gc} and P_iP phases. Reduction velocity is 6 km s^{-1} in all the record sections.

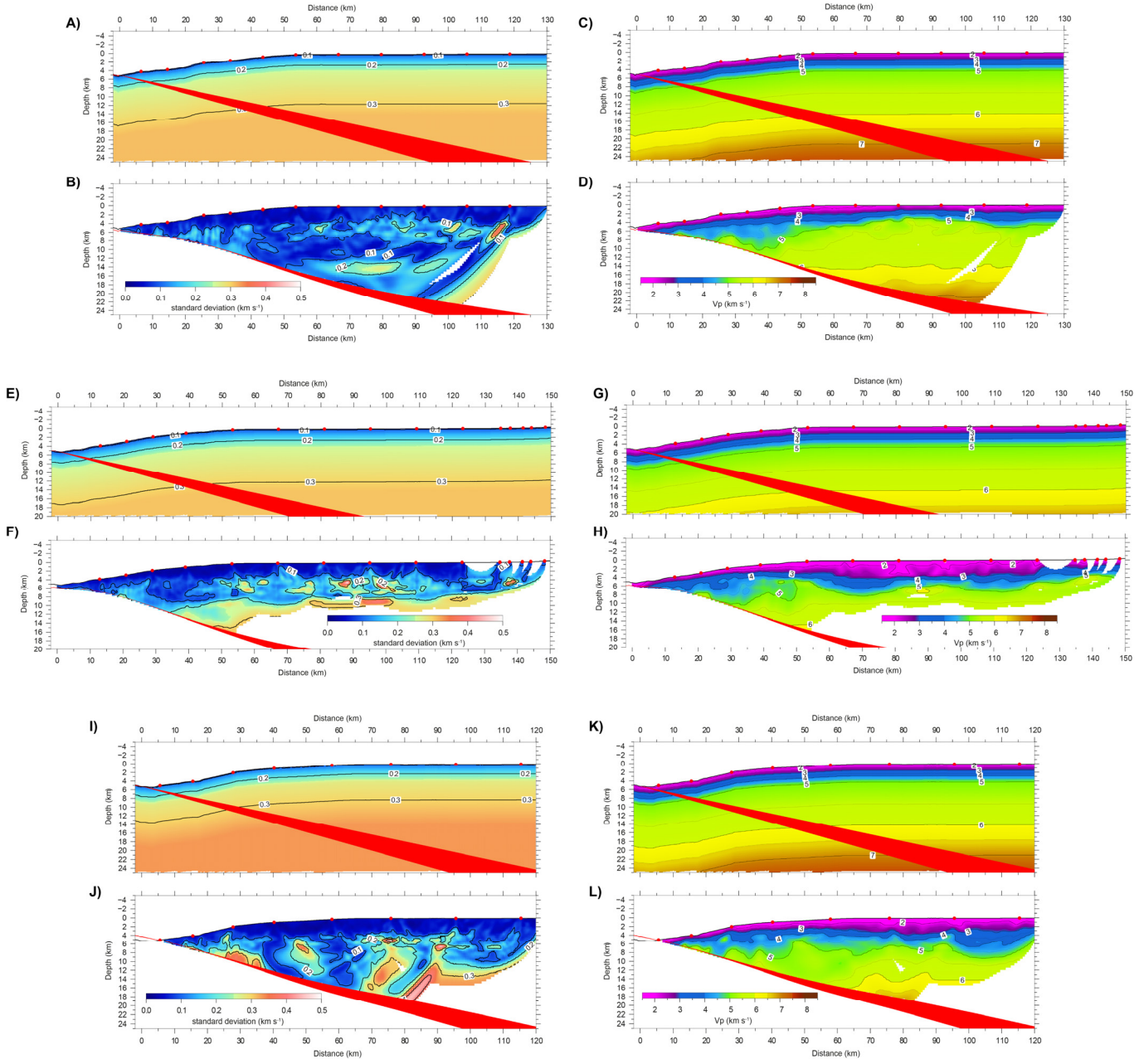

Fig. S7. Statistical analysis of inversion results. (A) Initial and **(B)** final standard deviation of the 100 Monte-Carlo realizations performed with NIC20 data. **(C)** Initial and **(D)** final averaged V_P model along NIC20. **(E)** Initial and **(F)** final standard deviation of the 100 Monte-Carlo realizations performed with NIC50 data. **(G)** Initial and **(H)** final averaged V_P model along NIC50. **(I)** Initial and **(J)** final standard deviation of the 100 Monte-Carlo realizations performed with NIC80/SO107 data. **(K)** Initial and **(L)** final averaged V_P model along NIC80/SO107. In all cases, red circles show OBH locations. The red band represents the standard deviation of the 100 Monte-Carlo realizations for the inter-plate reflector along the three profiles.

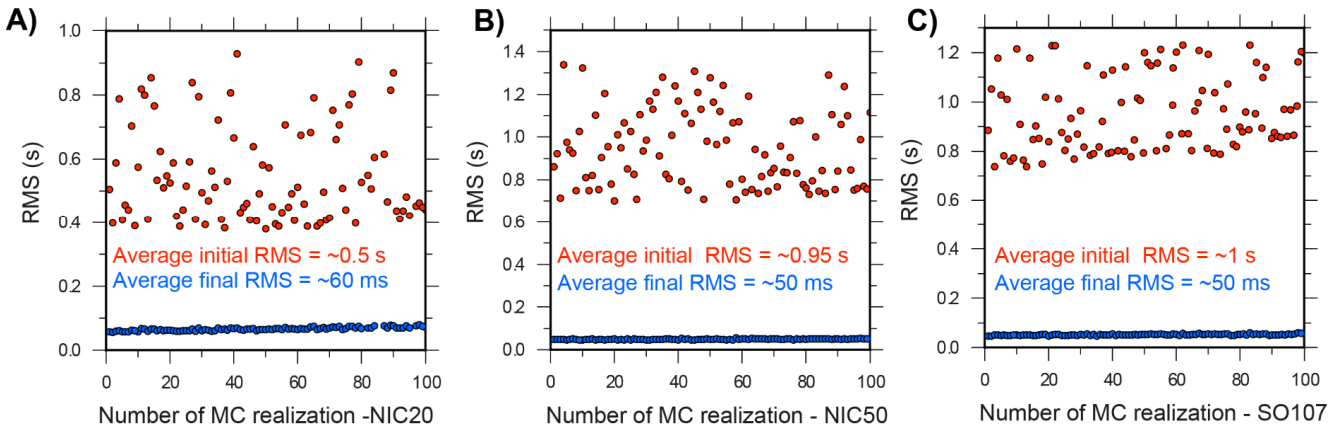

Fig. S8. Root mean square residuals before and after inversion. Initial (red circles) and final (blue circles) root mean square (RMS) travel-time residuals of the V_P seismic tomography models obtained along **(A)** NIC20, **(B)** NIC50, and **(C)** NIC80/SO107 profiles. The corresponding 2D V_P models are shown in Fig. 1B.

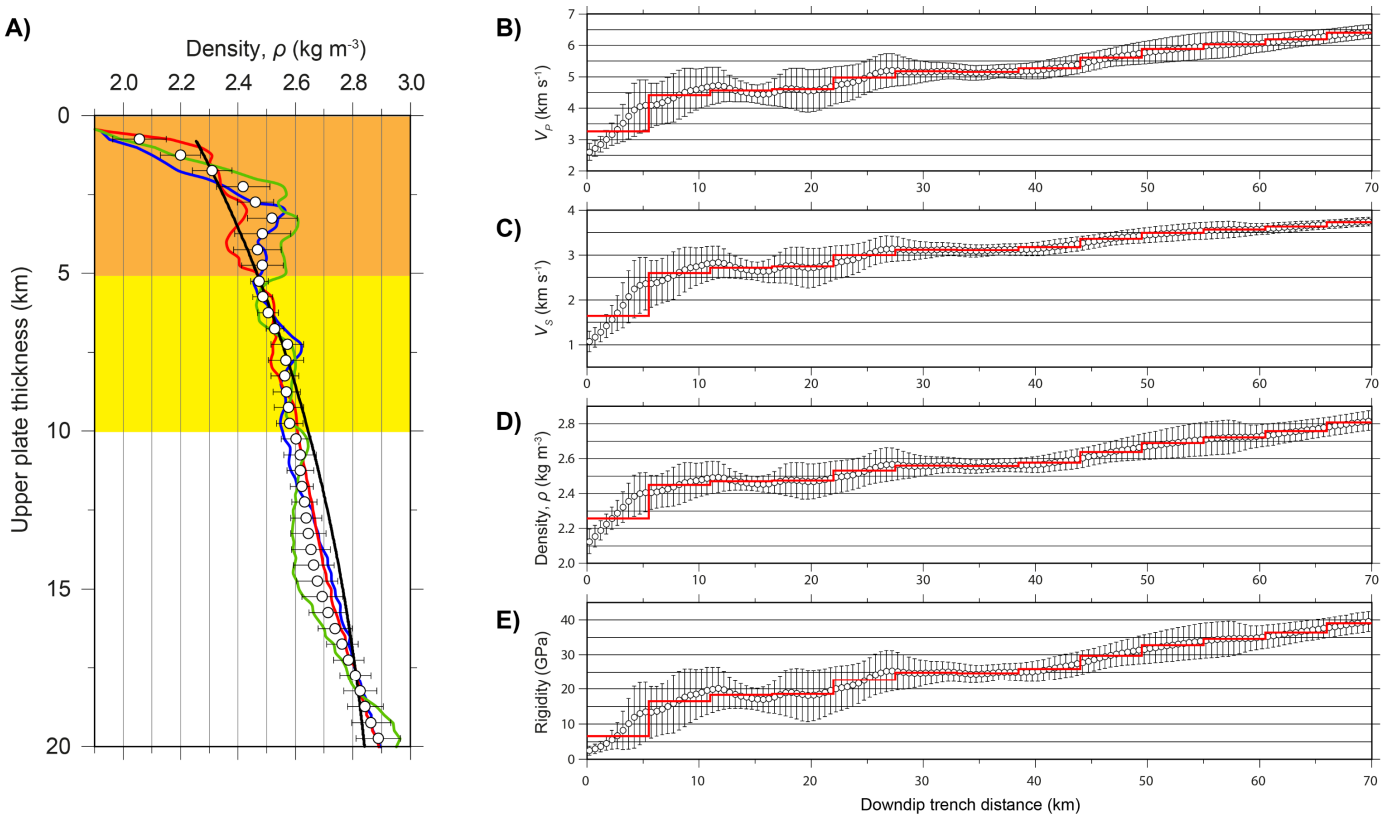

Fig. S9. Average upper-plate elastic rock properties. (A) $\rho(z)$ above the inter-plate boundary derived from the 2D V_P models in Fig. 1B applying Brocher's $\rho(V_P)$ empirical relationship (*46*). Green, blue and red colors correspond to the $\rho(z)$ values obtained at each profile in Fig. 1B following the color code in Fig. 3.The black line corresponds to the worldwide $\rho(z)$ average from Sallares and Ranero (*19*). White circles represent the average solution of the 100 Monte-Carlo realizations along the three profiles, and error bars represent the corresponding standard deviation. **(B)** V_P, **(C)**V_S, **(D)** ρ,**(E)** μ, as a function of downdip trench distance. White circles are the average of the three tomographic models and the error bars correspond to one standard deviation. Red line is the average value of each parameter within a 5.5 km-wide window.

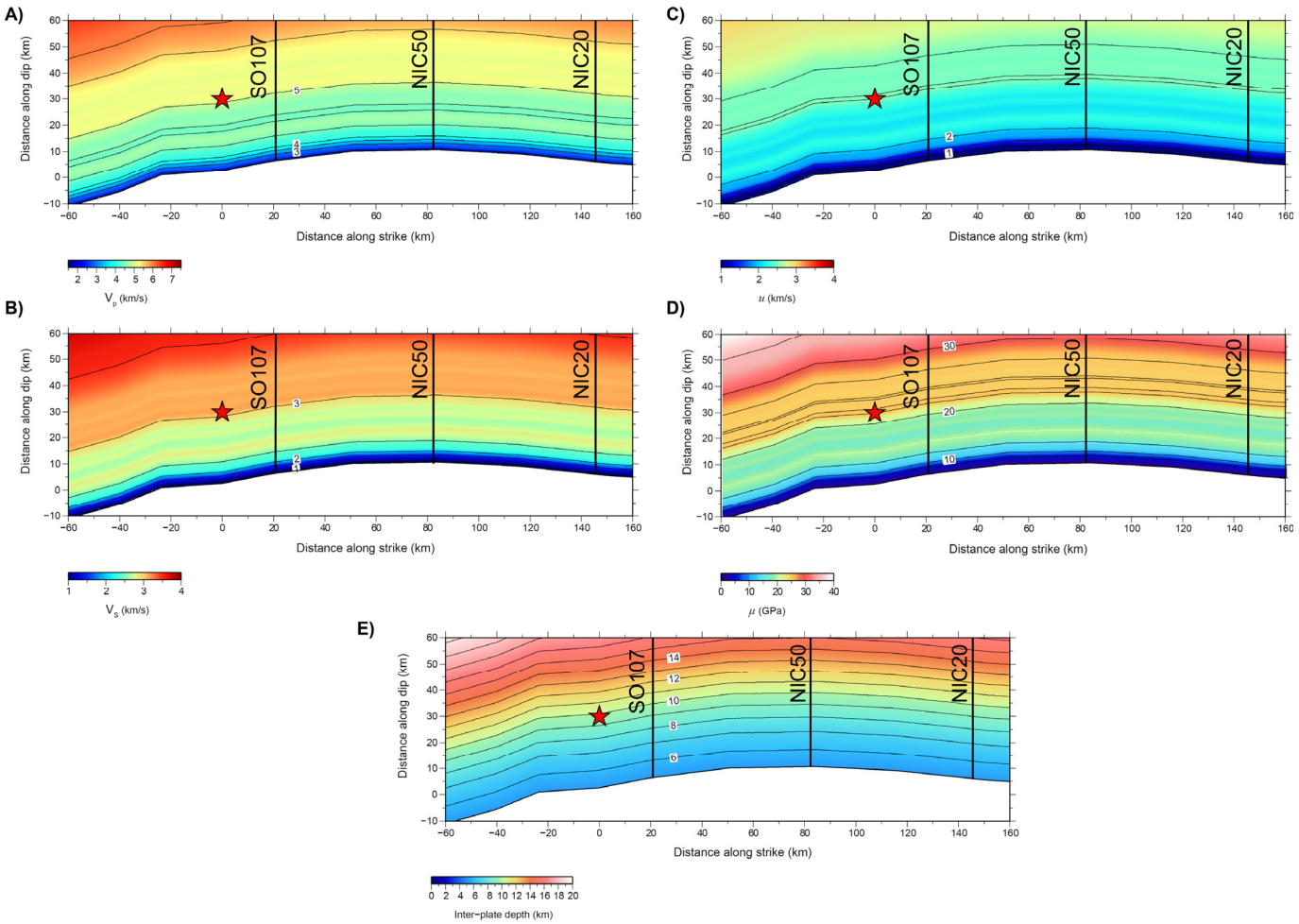

Fig. S10. 2D maps of elastic rock properties across the earthquake's rupture zone. The different panels show the spatial distribution of elastic properties above the inter-plate boundary throughout the rupture area of the Nicaragua 1992 tsunami earthquake obtained by extrapolation of the average values shown in Fig. 3. The different panels correspond to **(A)** V_P in km s^{-1} according to the color scale, **(B)** V_S in km s^{-1} according to the color scale, **(C)** u in km s^{-1} according to the color scale, **(D)** μ in GPa according to the color scale, **(E)** Inter-plate boundary depth below seafloor (bs) in *km* according to the color scale. The red star indicates the epicentral location of the event. Black lines show the location of the WAS seismic profiles.

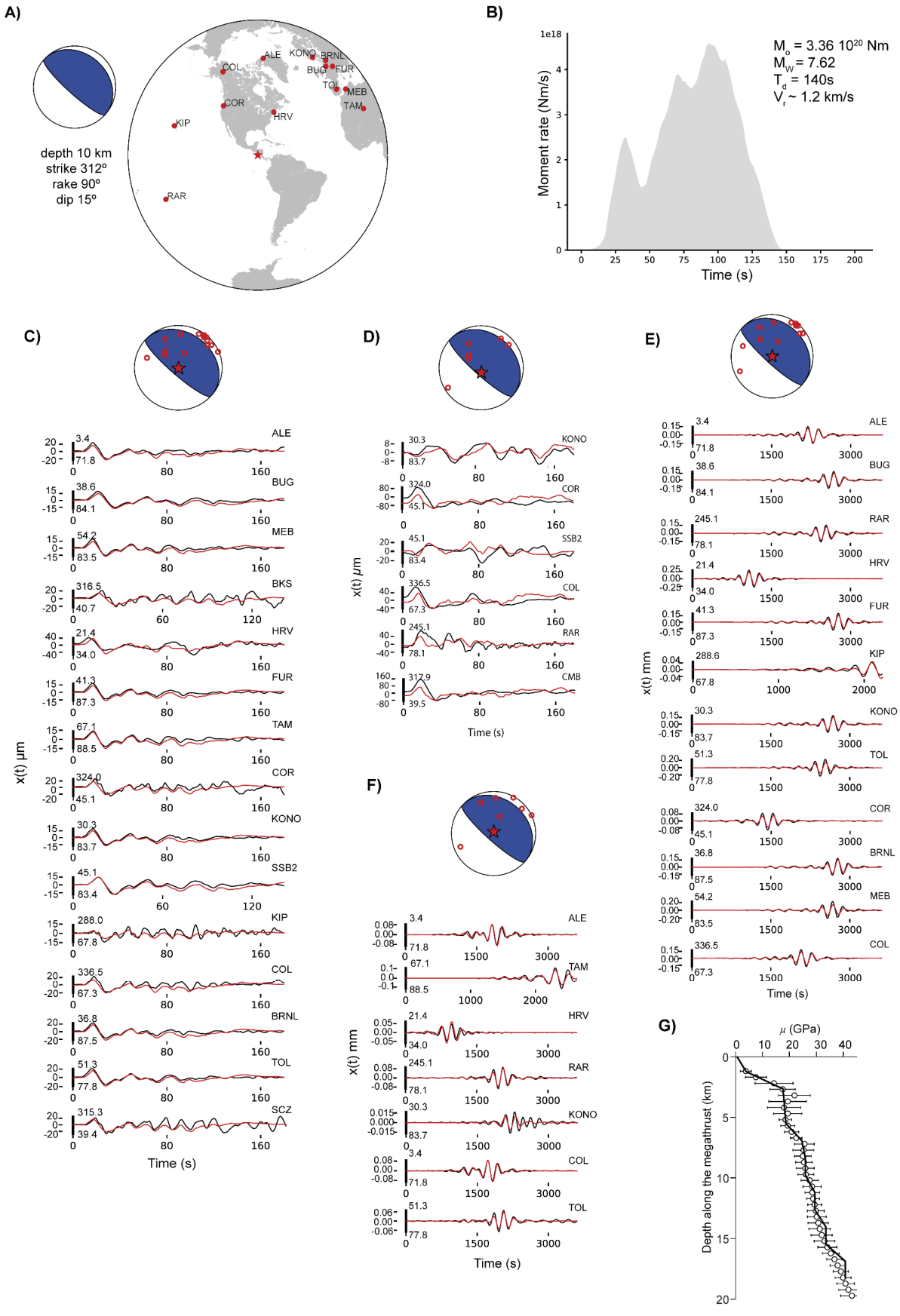
A)
depth 10 km
strike 312°
rake 90°
dip 15°
ALE
KONO
BRNL
COL
BUG
FUR
TOL
MEB
TAM
COR
HRV
KIP
RAR
B)
1e18
Moment rate (Nm/s)
Time (s)
M_o = 3.36 10^{20} Nm
M_W = 7.62
T_d = 140s
V_r ~ 1.2 km/s
C)
x(t) µm
ALE
BUG
MEB
BKS
HRV
FUR
TAM
COR
KONO
SSB2
KIP
COL
BRNL
TOL
SCZ
Time (s)
D)
x(t) µm
KONO
COR
SSB2
COL
RAR
CMB
Time (s)
E)
x(t) mm
ALE
BUG
RAR
HRV
FUR
KIP
KONO
TOL
COR
BRNL
MEB
COL
Time (s)
F)
x(t) mm
ALE
TAM
HRV
RAR
KONO
COL
TOL
Time (s)
G)
µ (GPa)
Depth along the megathrust (km)

(previous page)

Fig. S11. Finite fault inversion parameters of the Nicaragua 1992 earthquake. (A) Focal parameters of the seismic source used for the finite-fault inversion of the M_W7.62 1992 Nicaragua tsunami earthquake and map with the epicenter (red star) and station locations used in the inversion (red circles). **(B)** Inverted source-time function of the 1992 Nicaragua event. **(C)** Recorded (black line) and simulated (red line) P-waveform data at 15 teleseismic broadband stations. **(D)** Recorded (black line) and simulated (red line) SH waveforms at 6 broadband stations. **(E)** and **(F)** Recorded (black line) and simulated (red line) long period surface waves at 19 stations. **(G)** White circles with error bars are average 1D $\mu(z)$ –rigidity- values across the rupture zone of the Nicaragua 1992 earthquake derived from $V_P(z)$ models and their standard deviation (Fig. 3). The black line is the layered rigidity model used in the finite fault inversion, obtained by interpolation of the $\mu(z)$ model (white circles).

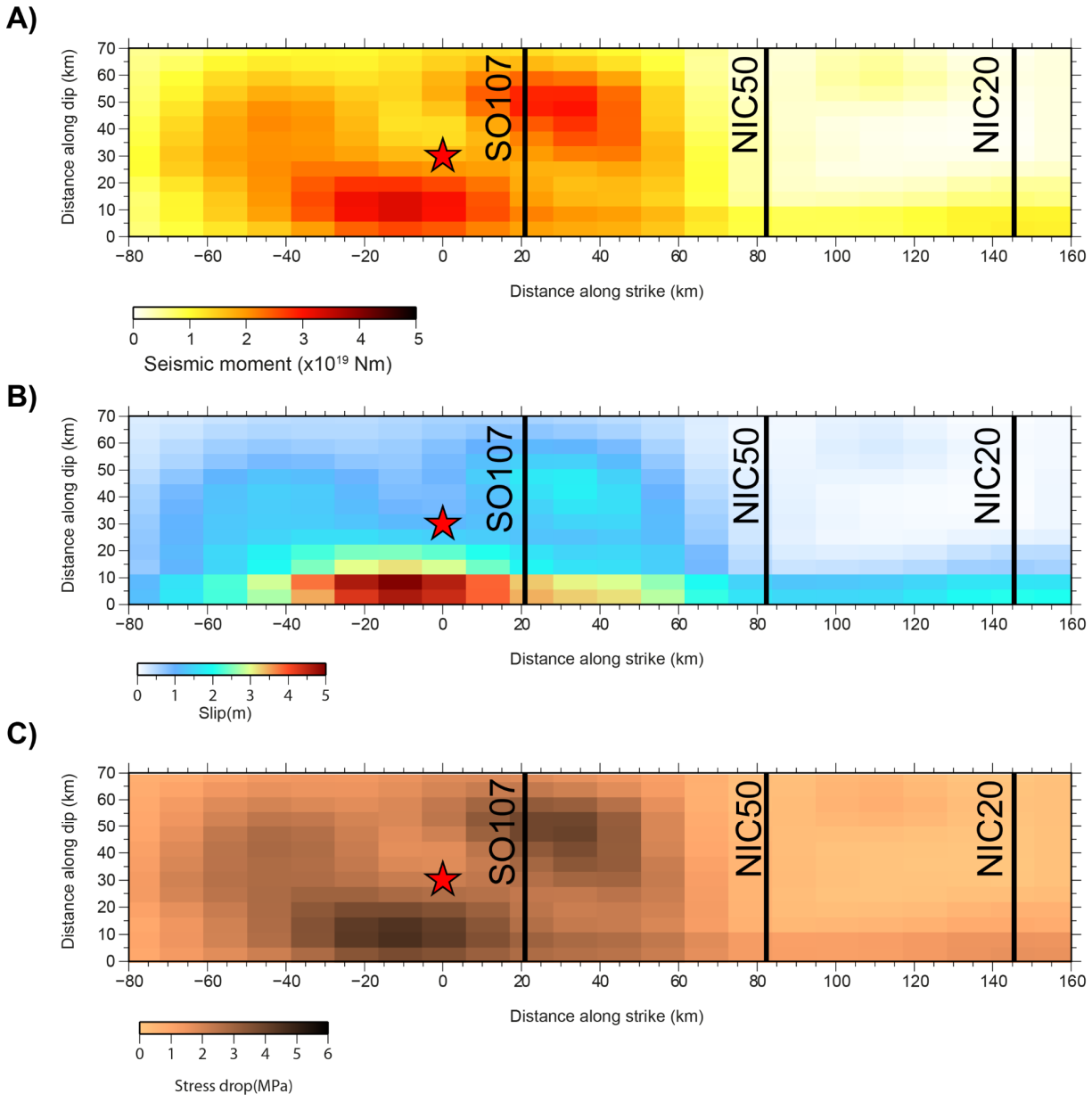

Fig. S12. Finite fault solution of the Nicaragua 1992 earthquake. The panels show maps of **(A)** seismic moment of the 1992 Nicaragua tsunami earthquake, according to the color scale, obtained in this work by finite fault inversion. Units are in Nm x10^{19}. **(B)** Co-seismic slip in *m,* according to the color scale, obtained in this work by finite fault inversion (see also Fig. S11). **(C)** Model-consistent stress drop distribution in *MPa*, according to the color scale, obtained in this work. In all cases, the grid cell size is 11x5.5 km. These grids have been smoothed out applying a 2D Delaunay triangulation filter to obtain the 2D maps in Fig. 4. The red star indicates the epicentral location used for this event (*34*). The vertical axis indicates downdip distance to the trench. Black lines show the location of the seismic profiles.